MAPK2 is a conserved Alveolate MAPK required for *Toxoplasma* cell cycle progression

Xiaoyu Hu[a], William J. O'Shaughnessy[a], Tsebaot G. Beraki[a], Michael L. Reese[a,b,#]

[a]Department of Pharmacology, University of Texas, Southwestern Medical Center, Dallas, Texas 75390-9041, USA

[b]Department of Biochemistry, University of Texas, Southwestern Medical Center, Dallas, Texas 75390-9041, USA

Running title: TgMAPK2 regulates centrosome duplication checkpoint

#Address correspondence to Michael L. Reese, michael.reese@utsouthwestern.edu

ORCIDs:

Michael Reese: 0000-0001-9401-9594

Keywords: kinase, cell cycle, centrosome, organelles

Abstract

Mitogen-activated protein kinases (MAPKs) are a conserved family of protein kinases that regulate signal transduction, proliferation, and development throughout eukaryotes. The Apicomplexan parasite *Toxoplasma gondii* expresses three MAPKs. Two of these, ERK7 and MAPKL1, have been respectively implicated in the regulation of conoid biogenesis and centrosome duplication. The third kinase, MAPK2, is specific to and conserved throughout Alveolata, though its function is unknown. We used the auxin-inducible degron system to determine phenotypes associated with MAPK2 loss-of-function in *Toxoplasma*. We found that parasites lacking MAPK2 were unable to replicate and arrested early in mitosis. While the parasites continued to replicate their mitochondria, apicoplasts, and Golgi apparatus, they failed to initiate daughter-cell budding, which ultimately led to parasite death. These phenotypes appear to be the result of a failure in centrosome duplication that is distinct from the MAPKL1 phenotype. As we did not observe MAPK2 localization at the centrosome at any point in the cell cycle, our data suggest MAPK2 regulates a process at a distal site that is required for completion of centrosome duplication.

Importance

Toxoplasma gondii is a ubiquitous intracellular protozoan parasite that can cause severe and fatal disease in immunocompromised patients and the developing fetus. Rapid parasite replication is critical for establishing a productive infection. Here, we demonstrate that a *Toxoplasma* protein kinase called MAPK2 is conserved throughout Alveolata and essential for parasite replication. We found that parasites lacking MAPK2 protein were defective in the initiation of daughter cell budding and were rendered inviable. Specifically, TgMAPK2 appears required for centrosome replication, and its loss causes arrest early in the cell cycle. MAPK2 is unique to Alveolata and not found in metazoa, and likely is a critical component of an essential parasite-specific signalling network.

Introduction

Cellular replication depends upon the faithful duplication and partition of genetic material and cell organelles. Successful progression through the eukaryotic cell cycle is controlled by a network of well-conserved regulatory components that not only organize different stages, but also adapt to extracellular signals (1). The obligate intracellular apicomplexan parasites have among the most diverse replicative paradigms among eukaryotes (2). These unusual cell cycles appear to be controlled by mechanisms both analogous to and divergent from their metazoan hosts (3–5). The *Toxoplasma gondii* asexual cycle replicates via "endodyogeny," wherein two daughters grow within an intact mother (6). Efficient replication of these parasites is critical to establishment of infection and also results in host tissue damage, thus contributing considerably to pathogenesis..

As the physical anchor for DNA segregation, the centrosome is central to the organization of cell division. Centrosome duplication is one of the earliest and most decisive events in the parasite cell cycle (3, 7–10). Earlier work identified two distinct centrosomal cores: an outer core and an inner core which orchestrate cytokinesis and nuclear division independently (3, 11). Daughter cell budding initiates prior to completion of mitosis, and the parasite centrosome is a central hub that coordinates both mitosis and daughter budding. Budding begins at the end of S phase with daughter cytoskeletal components assembling near the duplicated centrosomes, which provide a scaffold for daughter cell assembly (8, 12, 13). Organelles are then partitioned between these elongating scaffolds (14). A growing number of the regulatory components of the parasite cell cycle have been identified, including homologs of scaffolds (4, 15) and kinases (5, 8, 16, 17) that are broadly conserved in other organisms. However, the precise roles these factors play in *Toxoplasma* are often distinct from what they are known to play in model organisms – this is likely due to the parasite's specialized cell cycle (6) and unusual centrosomal structure (3, 11). Thus, even the study of well-conserved proteins can yield surprising insight into the functional adaptations evolved in the network that regulates the parasite cell cycle.

For example, throughout eukaryotes, members of the mitogen-activated protein kinase (MAPK)

family are essential regulators of cell proliferation and differentiation (18–21). The *Toxoplasma* genome encodes three MAPKs: ERK7, MAPKL1, and MAPK2 (Figure 1A). ERK7 is conserved throughout eukaryota and we have recently shown that TgERK7 is essential for conoid biogenesis (22). MAPKL1 is found only in coccidian parasites, and plays a role in preventing centrosome overduplication in order to ensure proper binary division through endodyogeny (3, 23). We have identified the cellular function of the third kinase, MAPK2, which is specific to and conserved throughout Alveolata. To uncover the function of MAPK2 in *Toxoplasma*, we applied the auxin-inducible degron (AID) system to inducibly degrade the protein. We found that parasites lacking TgMAPK2 arrested early in cell cycle, which eventually led to parasite death. These parasites failed to duplicate their centrosomes, and never initiated daughter cell budding, implicating TgMAPK2 as an essential regulator of an early check point in the *Toxoplasma* cell cycle.

Results

MAPK2 localizes to cytoplasmic puncta in Toxoplasma

The *Toxoplasma* genome encodes three MAPKs. Two of these kinases have been characterized: TgMAPKL1 (TGME49_312570) prevents centrosome overduplication (3) and TgERK7 (TGME49_233010) is required for conoid biogenesis (24, 25). The gene TGME49_207820 encodes the *Toxoplasma* ortholog of MAPK2, a MAPK that is specific to and conserved in all Alveolates, suggesting a specialized function (Figure 1A). We first sought to determine the subcellular localization of TgMAPK2. To this end, we engineered a parasite strain to express the native TgMAPK2 with a C-terminal 3xHA epitope tag (TgMAPK2^{3xHA}) using a CRISPR-mediated double homologous recombination strategy. A western blot of TgMAPK2^{3xHA} parasite lysate probed with anti-HA antibody showed a single band of the expected mass (66-kD; Figure 1B).

Our initial immunofluorescence analysis (IFA) revealed that TgMAPK2 appears as puncta dispersed throughout the parasite cytosol (Figure 2A). We therefore co-stained with anti-β-tubulin and several other well-characterized markers for parasite organelles. We observed no co-localization of

TgMAPK2^{3xHA} puncta with any organellar markers we tested (Figure 2A,B), including tubulin, Hoechst, the mitochondria (anti-TOM40), apicoplast (anti-ACP), rhoptries (anti-ROP2), or centrosome/conoid (Centrin 1 and Centrin 2). We reasoned that the TgMAPK2 puncta may represent intracellular vesicles and went on to test its co-localization with markers for intracellular trafficking including the Golgi (GRASP55) and endolysosomal trafficking system (*Toxoplasma* Rab proteins) (26). While many of these markers also appear punctate, confocal imaging revealed TgMAPK2^{3xHA} does not localize to structures stained by any of GRASP55, Rab5a, Rab6, or Rab7 (Figure 2). TgMAPK2 therefore appears to mark a structure that is distinct from well-characterized organelles and trafficking machinery in *Toxoplasma*. Moreover, we observed that the TgMAPK2 signal dropped to near undetectable levels late in the parasite cell cycle (Figure 2C). While this loss of signal intensity may be due to dissolution of the TgMAPK2 puncta, it is consistent with the variation in TgMAPK2 transcript levels over the parasite cell cycle (Figure 2D; (27)).

TgMAPK2 is essential for the completion of parasite lytic cycle

We were unable to obtain MAPK2 knockouts using either homologous recombination or CRISPR-mediated strategies, so we applied the AID system. The AID system allows the conditional degradation of target proteins upon addition of a small molecule auxin (indole-3-acetic acid; IAA), and has been recently adapted to *Toxoplasma* (28). We engineered a parasite strain in which the MAPK2 protein was expressed in-frame with an AID and 3xFLAG tag at the C-terminus in the background of RHΔ*ku80* expressing the rice TIR1 auxin response protein (TgMAPK2^{AID}). TgMAPK2 localization appeared unaffected by the addition of the AID tag (Figure 3A). We found that TgMAPK2^{AID} was rapidly degraded upon addition of 500 μM auxin indole-3-acetic acid (IAA); TgMAPK2 protein was undetectable by western-blot after 15 minutes of IAA treatment (Figure 3B). We will refer to parasites in which TgMAPK2 has been inducibly degraded as TgMAPK2$^{AID/IAA}$. While TgMAPK2^{AID} parasites produced normal plaque numbers, TgMAPK2$^{AID/IAA}$ parasites produced no plaques (Figure 3C). Thus TgMAPK2 is essential for the lytic cycle, which is consistent with our inability to genetically disrupt the TgMAPK2 gene.

Plaque assays report on the entire lytic cycle, comprising multiple rounds of invasion, replication, and egress. Degradation of TgMAPK2 did not significantly affect parasite invasion or egress from host cells (Figure 3D,E). TgMAPK2$^{AID/IAA}$ parasites did not, however, replicate normally. Instead, we observed that many TgMAPK2$^{AID/IAA}$ parasites were only able to undergo a single round of replication following treatment with 500 μM IAA for 20 hours, after which they arrested and showed an aberrant morphology under phase contrast microscopy (Figure 3F). While TgMAPK2^{AID} parasites replicated normally, more than 80% of the TgMAPK2$^{AID/IAA}$ vacuoles contained two enlarged, morphologically aberrant parasites. The remaining TgMAPK2$^{AID/IAA}$ vacuoles contained a single oversized parasite (Figure 3F). These data led us to hypothesize that TgMAPK2 plays a crucial role at an early stage in the parasite cell cycle.

TgMAPK2 knock-down arrests parasites prior to initiation of daughter cell budding

During acute infection, the *Toxoplasma* tachyzoite replicates by endodyogeny, in which two daughter cells are assembled within the mother (6). This mechanism of division requires that organellar biogenesis be tightly coupled to the cell cycle. The parasite cellular ultrastructure thus changes drastically as cell cycle progresses, which provides us with a number of markers that can easily distinguish cell cycle stages via fluorescent microscopy and electron microscopy.

In a normal culture, the *Toxoplasma* cell cycle is synchronized within individual vacuoles (29), but asynchronous among vacuoles in a population, even among parasites that have invaded at the same time. Because parasites divide asynchronously, at any given time the parasites in a population occupy all stages of the cell cycle. We therefore reasoned we could identify the point of arrest upon TgMAPK2 degradation by examining arrested parasites and determining which structures are lost during increasing times of growth in the presence of IAA. Here we used a set of fluorescent markers to classify the parasite cell cycle into three broad categories: (i) “Non-budding”, (ii) “Budding” and (iii) “Cytokinesis” (Figure 4A). To distinguish these categories, we chose as markers (i) the *Toxoplasma* inner membrane complex 1 (IMC1) which stains the mother outline and growing daughter scaffolds; (ii) Tubulin, which labels the subpellicular microtubules and conoids; and (iii) Hoechst, which labels

150 nuclear and plastid DNA. We engineered the TgMAPK2^{AID} strain to co-express IMC1-mVenus and mTFP1-α-tubulin. TgMAPK2^{AID} parasites were allowed to invade a fresh monolayer of fibroblasts for 2 hours, after which uninvaded parasites were washed off. Media was changed to +IAA after increasing 2 hour increments, and all parasites were grown for a total of 10 hours (Figure 4A,B). Parasites were then fixed and prepared for imaging.

155 We quantified the number of parasites in each rough stage of the cell cycle for increasing incubation time in +IAA media (Figure 4C). We observed that parasites grown without IAA were 79±2% non-budding, 19±2% budding, and 3±1% undergoing cytokinesis. As time in IAA increased, we observed a marked decrease in the number of parasites that were budding and undergoing cytokinesis. After of 6-8 hours of IAA treatment, 98±2% of the parasites were in a non-budding state.
160 Taken together, these data demonstrate that the arrest we observe due to degradation of TgMAPK2 is prior to initiation of daughter cell budding, after which TgMAPK2 does not appear essential for cell cycle.

A regulatory arrest in cell cycle should be reversible by restoration of the protein. Induced degradation of an AID-tagged protein can be reversed by washing-out IAA (Figure 4D and (30)). We
165 therefore asked whether the block we had observed in parasite cell cycle due to TgMAPK2 degradation was reversible. TgMAPK2^{AID} parasites were allowed to invade host fibroblasts, and then grown for 8 h in the presence or absence of IAA. Parasites were then allowed to either continue to grow in IAA for an additional 18 h, or the media was changed to -IAA before continued growth. Parasites were then fixed and imaged by phase contrast microscopy. As expected, TgMAPK2^{AID}
170 parasites grown continuously in IAA were arrested. Parasites that had been grown for only 8 h in IAA before wash-out, however, were indistinguishable from those that had been grown without IAA (Figure 4E,F). Thus, the block in the *Toxoplasma* cell cycle caused by TgMAPK2 degradation likely represents a checkpoint arrest.

Degradation of TgMAPK2 does not block replication of mitochondrion, apicoplast, or Golgi apparatus

175 We have demonstrated that degradation of TgMAPK2 appears to arrest the parasite cell cycle

prior to daughter cell budding. To better understand the nature of this arrest, we next sought to characterize the morphological changes to the parasite after this arrest. We used transmission electron microscopy (TEM) to compare the ultrastructure of TgMAPK2^{AID} parasites grown in the absence of presence of IAA for a short time (6 hours), which was sufficient to induce arrest (Figure 5). We observed well-formed daughter buds in ~20% of the asynchronously dividing TgMAPK2^{AID} parasites (Figure 5A), which is consistent with our IFA quantification (Figure 4). While the TgMAPK2$^{AID/IAA}$ parasites did not show obvious ultrastructural defects, daughter cell budding appeared completely blocked (Figure 5B), again consistent with our IFA quantification. We next examined parasites that were incubated for extended periods in IAA. After 20 hours of in IAA, the architecture of TgMAPK2$^{AID/IAA}$ parasites was misshapen, as evidenced by enlarged cells and loss of the parasite's distinctive shape (Figures 5E-H). In addition, we observed an over-duplication of many organelles, including the Golgi apparatus and apicoplasts (Figures 5E-H). Moreover, at these longer time points, we observed vacuoles containing enlarged residual bodies filled with organellar debris, even in vacuoles containing only a single (albeit misshapen) parasite (Figures 5E). IFA with markers for mitochondria (TOM40) and the apicoplast (ACP1) confirmed that TgMAPK2^{AID} parasites replicated normally and maintained a normal count of a single apicoplast and mitochondrion per parasite (Figure 6A). However, TgMAPK$^{AID/IAA}$ parasites continued to replicate their mitochondria and apicoplasts after their arrest, though without the formation of new daughter cell buds, these organelles failed to separate and partition (Figure 6B). In addition, we observed substantially weaker nuclear DAPI staining TgMAPK$^{AID/IAA}$ parasites grown for 20h in IAA (Figure 6B), consistent with poor cellular health.

TgMAPK2 degradation impairs centrosome duplication

An early, crucial event prior to *Toxoplasma* daughter cell budding is the duplication of the centrosome (8). Centriole duplication during the G1/S boundary of the cell cycle marks entry into the S phase and provides a spatial direction for the assembly of the daughter buds (31). Earlier work identified an unusual bipartite structure of the centrosome in *Toxoplasma* which includes two cores: the outer core, distal from nucleus, and the inner core, proximal to nucleus (3). These cores have

distinct protein compositions, by which they can be easily distinguished (3). We therefore checked whether the duplication of either centrosome core was compromised in TgMAPK2$^{AID/IAA}$ parasites. We engineered the TgMAPK2^{AID} strain to express an mVenus fusion to the centrosomal outer core protein TgCentrin1, and a 3xHA fusion to the centrosomal inner core protein TgCEP250L1. Freshly invaded parasites were grown in the presence or absence of IAA for 8 hours. Anti-HA was used to stain TgCEP250L1, and Hoechst 33342 was included to track the nuclear DNA. We quantified the percentage of vacuoles with two clearly separated centrosomes based on the outer core marker mVenus-TgCentrin1 signal. As expected, 45±2% of TgMAPK2^{AID} parasites grown in the absence of IAA had successfully duplicated both centrosomal cores (Figure 7A), consistent with published reports (5, 8). However, we found that 94±1% of TgMAPK2$^{AID/IAA}$ parasites contained only a single centrosome (Figure 7A), suggesting a profound defect in centrosomal duplication in parasites lacking TgMAPK2. Somewhat surprisingly, the Hoechst-stained nucleus in the +IAA parasites were barely visible as compared to the -IAA parasites, when imaged at the same microscope settings (Figure 7A). Thus, the low-Hoechst intensity phenotype occurs early after loss of TgMAPK2 and is not a secondary effect or artifact of prolonged growth in IAA. This phenotype suggests that DNA replication may also be inhibited in TgMAPK2$^{AID/IAA}$ parasites. Unfortunately, the over-replication of the apicoplast and its genome complicated our efforts to unambiguously quantify this phenotype.

Our data show that TgMAPK2 is required for replication of centrosomes. Intriguingly, loss-of-function of another member of the MAPK family, TgMAPKL1 also causes a defect in parasite centrosome replication (3). Notably, the previous study was performed using a temperature-sensitive mutant that necessitated studies at longer timescales (20 h at non-permissive temperature) and at which we observed secondary effects using the AID system with MAPK2. We therefore sought to directly compare the phenotypes caused by inducible degradation of each of the two MAPKs. To this end, we generated a TgMAPKL1^{AID} strain using the same strategy as we used for MAPK2. Freshly invaded TgMAPKL1^{AID} parasites expressing mVenus-Centrin1 were grown in the presence of IAA for 8 hours. Parasites were fixed and stained with anti-TgIMC1. Consistent with published data (3), and in

contrast to the TgMAPK2$^{AID/IAA}$ phenotype, we observed that ~20% of the TgMAPKL1$^{AID/IAA}$ parasites had overduplicated both their centrosomes and daughter buds (Figure 7B). Thus these two divergent MAPKs both regulate centrosome replication even though they have opposing phenotypes, and are thus likely control different checkpoints in the *Toxoplasma* cell cycle.

Discussion

We have identified TgMAPK2 as essential to progressing through an early checkpoint in the *Toxoplasma* cell cycle. Our data demonstrate that without TgMAPK2, parasites arrest before centrosome duplication, causing a block in the initiation of parasite budding, and eventual parasite death. Intriguingly, organelles, including the Golgi apparatus, apicoplast, and mitochondria all continue to replicate, and relative parasite size increases, even though budding does not occur. The process of endodyogeny has historically been described as a careful coordination of organellar biogenesis with parasite budding (6, 14, 32). Our data suggest that organelle biogenesis is not directly coupled to cell cycle through regulatory checkpoints, but rather through simple timing. This idea is borne out by the ability to produce otherwise normal parasites in which the apicoplast does not replicate (33, 34). In addition, while the residual body is usually first observed after the first round of replication (35), and has recently been linked to inter-parasite trafficking within a vacuole (29), we observed enlarged residual bodies in vacuoles containing single, arrested parasites after long-term (20 h) MAPK2 degradation. Our data are therefore consistent with the role of the residual body in response to cellular stress.

A number of kinases with orthologs in model organisms have been identified as critical to the *Toxoplasma* cell cycle. These include kinases in the CDK (5, 16), Aurora (17, 36), and NEK (8) families. Progression through G1/S is a critical control point throughout eukaryota, and parasite kinases appear to perform similar functions to their metazoan orthologs in regulating this checkpoint. Notably, TgCRK1, an ortholog of metazoan CDK11, appears to regulate the transcriptional program that allows progress through the G1 checkpoint and centrosome duplication (5). In addition, TgNEK-1 is essential for centrosome separation (8). However, the ortholog of its mammalian substrate,

CEP250, does not appear to be a substrate of TgNEK-1. In fact, CEP250 and TgNEK-1 show distinct phenotypes upon disruption (4). Thus, while phylogenetically orthologous proteins to those in well-studied models exist in apicomplexan parasites, they may not be *functionally* orthologous.

In addition to well-conserved kinases, there are a number of Apicomplexa-specific members of many families that typically control the eukaryotic cell cycle (5, 37, 38). In *Toxoplasma*, these include two specialized MAPKs. MAPKL1 is found exclusively in coccidian organisms, which all replicate by endodyogeny during their asexual cycles. MAPK2 is conserved among all extant Alveolata for which genomes are available. While TgMAPKL1 localizes exclusively to the centrosome and prevents its overduplication (3), we have found that TgMAPK2 is required to complete a single round of centrosome duplication. We also found that TgMAPK2 never localizes to the centrosome, nor to the nucleus. It thus seems likely that TgMAPK2 regulates centrosome duplication indirectly, by controlling another process at a distal site that must be completed to progress through this checkpoint. The one unifying feature of all Alveolate organisms is the membrane and cytoskeletal structure known as the inner membrane complex (IMC) in Apicomplexa, and as “alveoli” in other organisms. The processes that regulate and drive the IMC biogenesis are still a mystery. However, the IMC forms the scaffold for new daughter cells (6, 39), a process that occurs concurrently with centrosome duplication (8–10, 12, 39), Given its evolutionary history, it is intriguing to hypothesize that TgMAPK2 plays a role in the crosstalk between these two processes.

Materials and Methods

Sequence analysis and phylogeny. Protein sequences for kinases were obtained from ToxoDBv43 and Uniprot. The kinase domains were aligned using MAFFT (40), and the resulting alignments were used to estimate the maximum likelihood phylogenetic tree with bootstrap analysis (1000 replicates) in IQ-tree v1.6.12 (41, 42), with the gamma-corrected empirical-frequency LG substitution model.

PCR and plasmid generation. All PCRs were conducted using Q5 DNA polymerase (New England Biolabs) and the primers listed in Supplemental Table 1. Constructs were assembled using Gibson master mix (New England Biolabs).

Parasite culture and transfection. Human foreskin fibroblasts (HFFs) were grown in DMEM supplemented with 10% fetal bovine serum and 2 mM glutamine. *Toxoplasma* tachyzoites were maintained in confluent monolayers of HFF. TgMAPK^{3xHA} and TgMAPK2^{AID} strains were generated by transfecting the RH*Δku80Δhxgprt* strain (43) or the same strain expressing OsTIR1 driven by the gra1-promoter (24). Transfections included a Cas9/CRISPR vector targeting the TgMAPK2 3' and a Q5 PCR product with 500 bp homology arms flanking the appropriate tag. mTFP1-α-Tubulin, GFP-α-Tubulin, TgIMC1-mVenus, mVenus-TgCentrin1 expressing parasites were created by amplifying the FP-marker expression cassette and an adjacent chloramphenicol (or HXGPRT) resistance cassette by PCR and targeting it to a site adjacent Ku80 locus by CRISPR/Cas9-mediated homologous recombination (see Supplemental Table S1) and selecting with chloramphenicol. TgCEP250L1^{3xHA} parasite was generated by C-terminal single homologous recombination as described (4). The original pTub and pMIN vector was a kind gift of Ke Hu (University of Indiana). The original GRASP-GFP, Neon-Rab5a, EmFP-Rab6, Neon-Rab7, Emerald-Centrin1 and eGFP-Centrin2 was a kind gift of Aoife Heaslip (University of Connecticut).

Western blotting. Proteins were separated by SDS–PAGE and transferred to a polyvinylidene difluoride membrane. Membranes were blocked for 1 h in PBS + 5% milk, followed by overnight incubation at 4°C with primary antibody in blocking solution. The next day, membranes were washed three times with TBST, followed by incubation at room temperature for 1–2 h with HRP-conjugated

secondary antibody (Sigma) in blocking buffer. After three washes with TBST, Western blots were imaged using ECL Plus reagent (Pierce) on a GE ImageQuant LAS4000. Antibodies used in this study include Rb anti-β-tubulin (1:10000 dilution), rat anti-HA (Sigma; 1:1000 dilution), and mouse m2 anti-FLAG (Sigma; 1:1000 dilution).

Immunofluorescence and fluorescence colocalization quantification. HFF cells were grown on coverslips in 24-well plates until confluent and were infected with parasites. The cells were rinsed twice with phosphate buffered saline (PBS), and were fixed with 4% paraformaldehyde (PFA)/4% sucrose in PBS at room temperature for 15 min. After two washes with PBS, cells were permeabilized with 0.1% Triton X-100 for 15 min and washed three times with PBS. After blocking in PBS + 3% bovine serum albumin for 30 min, cells were incubated in primary antibody in blocking solution overnight at room temperature. Cells were then washed three times with PBS and incubated with Alexa-Fluor conjugated secondary antibodies (Molecular Probes) for 2 h. Cells were then washed three times with PBS and then mounted with mounting medium containing DAPI (Vector Laboratories). For tyramide amplification of TgMAPK2^{AID}-3xFLAG signal, the above protocol was altered as follows. Endogenous peroxidase activity was quenched by incubation of fixed coverslips with 100 mM sodium azide in PBS for 45 min at room temperature. Cells were blocked with 5% horse serum/0.5% Roche Western Blocking Reagent in TBST for 45 min. HRP-conjugated goat anti-mouse secondary antibody (Sigma) was used and tyramide-fluorophore was allowed to react for 30 s before final washes. Cells were imaged on either a Nikon A1 Laser Scanning Confocal Microscope or a Nikon Ti2E wide-field microscope. Primary antibodies used in this study include rat anti-HA 3F10 (Roche #11867423001), mouse m2 anti-FLAG (Sigma #F1804), rabbit anti-β-tubulin (1:10,000 dilution), rabbit anti-TOM40 (1:2,000 dilution), rabbit anti-ACP (1:2,000 dilution), rabbit anti-ROP2 (1:10,000 dilution), mouse MAb 45.36 anti-TgIMC1 (1:2,000 dilution, a generous gift from Gary Ward, The University of Vermont). Pearson's coefficient was calculated for all the Z-stacks of the images of a minimum of 20 cells using Coloc 2 software in ImageJ. Quantification of signal overlap between the fluorescent signals between TgMAPK2^{3xHA} and each of the markers depicted in the figure 2B, mean ± SD.

Plaque assay. Plaque assays were performed using 6-well plates containing HFFs infected with 200 parasites per well in the presence or absence of 500 μM IAA. After 7 days, the cells were fixed with methanol, stained with crystal violet solution, and the resulting plaques were counted. All plaques assays were performed in biological triplicate.

Transmission electron microscopy. Cells were fixed on MatTek dishes with 2.5% (vol/vol) glutaraldehyde in 0.1 M sodium cacodylate buffer. After three rinses in 0.1 M sodium cacodylate buffer, they were postfixed with 1% osmium tetroxide and 0.8% K3[Fe(CN6)] in 0.1 M sodium cacodylate buffer for 1 h at room temperature. Cells were rinsed with water and en bloc stained with 2% aqueous uranyl acetate overnight. After three rinses with water, specimens were dehydrated with increasing concentration of ethanol, infiltrated with Embed-812 resin, and polymerized in a 70°C oven overnight. Blocks were sectioned with a diamond knife (Diatome) on a Leica Ultracut UC7 ultramicrotome (Leica Microsystems) and collected onto copper grids, poststained with 2% uranyl acetate in water and lead citrate. All TEM images were acquired on a Tecnai G2 spirit transmission electron microscope (FEI) equipped with a LaB6 source at 120 kV. Images in Figure 5B of sectioned cells are representative of 15 TgMAPK2^{AID}, 40 TgMAPK2$^{AID/IAA}$ (6h IAA duration) and 40 TgMAPK2$^{AID/IAA}$ (20h IAA duration) vacuoles. The numbers of Golgi per parasite were counted manually from 35 images.

Invasion and egress assay. Invasion and egress assays were performed using mTFP1-α-Tubulin expressed TgMAPK2^{AID} parasites. Parasites were allowed to grow overnight without IAA. The next day, 2 h before the assay was initiated, media was switched to IAA (or mock) media. Parasites were mechanically released from host cells, and 2×10^6 parasites of each condition were added to confluent HFFs grown on coverslips in a 24 well plate, where they were allowed to invade at 37°C for 2 h in -/+ IAA media. These were then washed 10x with PBS, fixed, and attached parasites were stained with anti-SAG1 without permeabilization. Assays were conducted in biological triplicates each of technical triplicates. The mTFP1-α-Tubulin positive but SAG1 negative parasites were regarded as internal (invaded) parasites. To measure egress, parasites were grown for 24–30 h in confluent HFFs on coverslips. 2 h before the assay was initiated, media was switched to IAA, as above. Cells were

washed with prewarmed Hank's balanced salt solution (HBSS) before the assay, and then incubated with HBSS containing 3 μM calcium ionophore A23187 (Cayman Chemical) for 1 min at 37°C before fixation and imaging.

Statistical analysis and figure generation. Statistical tests were conducted in GraphPad Prism v8.4. All shown are mean and error bars indicate S.D. Images were analyzed using the Fiji distribution of ImageJ (44). Figures were created using Inkscape v0.92.

Acknowledgments

We thank Melanie Cobb and members of the Cobb and Reese labs for lively discussions; the UT Southwestern Electron Microscopy core facility for assistance with data collection. M.L.R. acknowledges funding from the Welch Foundation (I-1936-20170325), National Science Foundation (MCB1553334), and National Institutes of Allergy and Infectious Disease (R01AI150715). X.H. was funded, in part, by Cancer Prevention and Research Institute of Texas Training Grant RP160157. T.B. was funded, in part, by NIH training grant T32GM008203.

References

1. Harashima H, Dissmeyer N, Schnittger A. 2013. Cell cycle control across the eukaryotic kingdom. Trends Cell Biol 23:345–356.

2. Francia ME, Striepen B. 2014. Cell division in apicomplexan parasites. Nat Rev Microbiol 12:125–136.

3. Suvorova ES, Francia M, Striepen B, White MW. 2015. A novel bipartite centrosome coordinates the apicomplexan cell cycle. PLoS Biol 13:e1002093.

4. Chen C-T, Gubbels M-J. 2019. TgCep250 is dynamically processed through the division cycle and is essential for structural integrity of the Toxoplasma centrosome. Mol Biol Cell 30:1160–1169.

5. Alvarez CA, Suvorova ES. 2017. Checkpoints of apicomplexan cell division identified in Toxoplasma gondii. PLoS Pathog 13:e1006483.

6. Hu K, Mann T, Striepen B, Beckers CJM, Roos DS, Murray JM. 2002. Daughter cell assembly in the protozoan parasite Toxoplasma gondii. Mol Biol Cell 13:593–606.

7. Blader IJ, Coleman BI, Chen C-T, Gubbels M-J. 2015. Lytic Cycle of Toxoplasma gondii: 15 Years Later. Annu Rev Microbiol 69:463–485.

8. Chen C-T, Gubbels M-J. 2013. The Toxoplasma gondii centrosome is the platform for internal daughter budding as revealed by a Nek1 kinase mutant. J Cell Sci 126:3344–3355.

9. Brooks CF, Francia ME, Gissot M, Croken MM, Kim K, Striepen B. 2011. Toxoplasma gondii sequesters centromeres to a specific nuclear region throughout the cell cycle. Proc Natl Acad Sci U S A 108:3767–3772.

10. Striepen B, Crawford MJ, Shaw MK, Tilney LG, Seeber F, Roos DS. 2000. The plastid of Toxoplasma gondii is divided by association with the centrosomes. J Cell Biol 151:1423–1434.

11. Morlon-Guyot J, Francia ME, Dubremetz J-F, Daher W. 2017. Towards a molecular architecture of the centrosome in Toxoplasma gondii. Cytoskeleton 74:55–71.

12. Anderson-White BR, Ivey FD, Cheng K, Szatanek T, Lorestani A, Beckers CJ, Ferguson DJP, Sahoo N, Gubbels M-J. 2011. A family of intermediate filament-like proteins is sequentially assembled into the cytoskeleton of Toxoplasma gondii. Cell Microbiol 13:18–31.

13. Agop-Nersesian C, Egarter S, Langsley G, Foth BJ, Ferguson DJP, Meissner M. 2010. Biogenesis of the inner membrane complex is dependent on vesicular transport by the alveolate specific GTPase Rab11B. PLoS Pathog 6:e1001029.

14. Nishi M, Hu K, Murray JM, Roos DS. 2008. Organellar dynamics during the cell cycle of Toxoplasma gondii. J Cell Sci 121:1559–1568.

15. Francia ME, Jordan CN, Patel JD, Sheiner L, Demerly JL, Fellows JD, de Leon JC, Morrissette NS, Dubremetz J-F, Striepen B. 2012. Cell division in Apicomplexan parasites is organized by a homolog of the striated rootlet fiber of algal flagella. PLoS Biol 10:e1001444.

16. Naumov A, Kratzer S, Ting L-M, Kim K, Suvorova ES, White MW. 2017. The Toxoplasma Centrocone Houses Cell Cycle Regulatory Factors. mBio 8.

17. Berry L, Chen C-T, Reininger L, Carvalho TG, El Hajj H, Morlon-Guyot J, Bordat Y, Lebrun M, Gubbels M-J, Doerig C, Daher W. 2016. The conserved apicomplexan Aurora kinase TgArk3 is involved in endodyogeny, duplication rate and parasite virulence. Cell Microbiol 18:1106–1120.

18. Boulton TG, Yancopoulos GD, Gregory JS, Slaughter C, Moomaw C, Hsu J, Cobb MH. 1990. An insulin-stimulated protein kinase similar to yeast kinases involved in cell cycle control. Science 249:64–67.

19. Sasabe M, Machida Y. 2012. Regulation of organization and function of microtubules by the mitogen-activated protein kinase cascade during plant cytokinesis. Cytoskelet Hoboken NJ

69:913–918.

20. Schwebs DJ, Hadwiger JA. 2015. The Dictyostelium MAPK ERK1 is phosphorylated in a secondary response to early developmental signaling. Cell Signal 27:147–155.

21. Zhang Y, Wang P, Shao W, Zhu J-K, Dong J. 2015. The BASL polarity protein controls a MAPK signaling feedback loop in asymmetric cell division. Dev Cell 33:136–149.

22. O'Shaughnessy WJ, Hu X, Beraki T, McDougal M, Reese ML. 2020. Loss of a conserved MAPK causes catastrophic failure in assembly of a specialized cilium-like structure in Toxoplasma gondii. Mol Biol Cell 31:881–888.

23. Sugi T, Kawazu S-I, Horimoto T, Kato K. 2015. A single mutation in the gatekeeper residue in TgMAPKL-1 restores the inhibitory effect of a bumped kinase inhibitor on the cell cycle. Int J Parasitol Drugs Drug Resist 5:1–8.

24. O'Shaughnessy WJ, Hu X, McDougal M, Reese ML. Loss of a conserved MAPK causes catastrophic failure in assembly of a specialized cilium-like structure in Toxoplasma gondii. bioRxiv.

25. Back PS, O'Shaughnessy WJ, Moon AS, Dewangan PS, Hu X, Sha J, Wohlschlegel JA, Bradley PJ, Reese ML. 2020. Ancient MAPK ERK7 is regulated by an unusual inhibitory scaffold required for Toxoplasma apical complex biogenesis. bioRxiv 10.1101/2020.02.02.931089.

26. Kremer K, Kamin D, Rittweger E, Wilkes J, Flammer H, Mahler S, Heng J, Tonkin CJ, Langsley G, Hell SW, Carruthers VB, Ferguson DJP, Meissner M. 2013. An overexpression screen of Toxoplasma gondii Rab-GTPases reveals distinct transport routes to the micronemes. PLoS Pathog 9:e1003213.

27. Behnke MS, Wootton JC, Lehmann MM, Radke JB, Lucas O, Nawas J, Sibley LD, White MM. 2010. Coordinated progression through two subtranscriptomes underlies the tachyzoite cycle of

Toxoplasma gondii. PLoS One 5:e12354.

28. Brown KM, Long S, Sibley LD. 2017. Plasma Membrane Association by N-Acylation Governs PKG Function in Toxoplasma gondii. mBio 8.

29. Periz J, Whitelaw J, Harding C, Gras S, Del Rosario Minina MI, Latorre-Barragan F, Lemgruber L, Reimer MA, Insall R, Heaslip A, Meissner M. 2017. Toxoplasma gondii F-actin forms an extensive filamentous network required for material exchange and parasite maturation. eLife 6.

30. Holland AJ, Fachinetti D, Han JS, Cleveland DW. 2012. Inducible, reversible system for the rapid and complete degradation of proteins in mammalian cells. Proc Natl Acad Sci 109:E3350–E3357.

31. Gubbels M-J, White M, Szatanek T. 2008. The cell cycle and Toxoplasma gondii cell division: tightly knit or loosely stitched? Int J Parasitol 38:1343–1358.

32. Sheffield HG, Melton ML. 1968. The Fine Structure and Reproduction of Toxoplasma gondii. J Parasitol 54:209–226.

33. Fichera ME, Roos DS. 1997. A plastid organelle as a drug target in apicomplexan parasites. 6658. Nature 390:407–409.

34. He CY, Shaw MK, Pletcher CH, Striepen B, Tilney LG, Roos DS. 2001. A plastid segregation defect in the protozoan parasite Toxoplasma gondii. EMBO J 20:330–339.

35. Attias M, Miranda K, De Souza W. 2019. Development and fate of the residual body of Toxoplasma gondii. Exp Parasitol 196:1–11.

36. Berry L, Chen C-T, Francia ME, Guerin A, Graindorge A, Saliou J-M, Grandmougin M, Wein S, Bechara C, Morlon-Guyot J, Bordat Y, Gubbels M-J, Lebrun M, Dubremetz J-F, Daher W. 2018. Toxoplasma gondii chromosomal passenger complex is essential for the organization of a functional mitotic spindle: a prerequisite for productive endodyogeny. Cell Mol Life Sci CMLS

75:4417–4443.

37. Talevich E, Mirza A, Kannan N. 2011. Structural and evolutionary divergence of eukaryotic protein kinases in Apicomplexa. BMC Evol Biol 11:321.

38. Peixoto L, Chen F, Harb OS, Davis PH, Beiting DP, Brownback CS, Ouloguem D, Roos DS. 2010. Integrative genomic approaches highlight a family of parasite-specific kinases that regulate host responses. Cell Host Microbe 8:208–218.

39. Anderson-White B, Beck JR, Chen C-T, Meissner M, Bradley PJ, Gubbels M-J. 2012. Cytoskeleton assembly in Toxoplasma gondii cell division. Int Rev Cell Mol Biol 298:1–31.

40. Katoh K, Standley DM. 2013. MAFFT multiple sequence alignment software version 7: improvements in performance and usability. Mol Biol Evol 30:772–780.

41. Minh BQ, Schmidt HA, Chernomor O, Schrempf D, Woodhams MD, von Haeseler A, Lanfear R. 2020. IQ-TREE 2: New Models and Efficient Methods for Phylogenetic Inference in the Genomic Era. Mol Biol Evol 37:1530–1534.

42. Hoang DT, Chernomor O, von Haeseler A, Minh BQ, Vinh LS. 2018. UFBoot2: Improving the Ultrafast Bootstrap Approximation. Mol Biol Evol 35:518–522.

43. Huynh M, Carruthers VB. 2009. Tagging of endogenous genes in a Toxoplasma gondii strain lacking Ku80. Eukaryot Cell 8:530–9.

44. Schindelin J, Arganda-Carreras I, Frise E, Kaynig V, Longair M, Pietzsch T, Preibisch S, Rueden C, Saalfeld S, Schmid B, Tinevez J-Y, White DJ, Hartenstein V, Eliceiri K, Tomancak P, Cardona A. 2012. Fiji: an open-source platform for biological-image analysis. Nat Methods 9:676–682.

Figure Legends

365 **Figure 1.** (A) Phylogenetic tree demonstrates MAPK2 represents a distinct MAPK subfamily

(highlighted purple) that is conserved throughout Alveolata. Human MAPKs ERK1, ERK5, JNK1, and p38 are highlighted orange. Human DYRK1, GSK3, and ERK7 and *Toxoplasma* MAPKL1 and ERK7 were used as outgroups. Bootstrap support indicated by: Black circles >95%; Open circles >80%. (B) Western blot on TgMAPKL2^{3xHA} and parental lysates. β-Tubulin (anti-β-Tubulin) was used as a loading control.

Figure 2. TgMAPK2 forms cytosolic puncta in interphase and early budding parasites. (A) 0.5-µm confocal slices of TgMAPK2^{3xHA} and GFP-α-Tubulin (blue) expressing parasites were either stained or transiently transfected (Centrin and Rab FP fusions) with the indicated markers. (B) Pearson's correlation coefficients for TgMAPK2^{3xHA} and the indicated markers from (A); n=20 cells. (C) TgMAPK2^{3xHA} intensity diminishes late in the cell cycle. (D) Transcript levels of MAPK2 peak during G1/early S (data (27), retrieved from ToxoDBv43). All scale bars: 5 µm.

Figure 3. TgMAPK2 is essential for parasite proliferation. (A) 0.5-µm confocal slice of TgMAPK2^{AID} parasites using anti-FLAG (green) and anti-β-Tubulin (magenta). Scale bar = 5 µm. (B) Western blot of TgMAPK2^{AID} protein levels at increasing growth time in 500 µM IAA. Anti-β-tubulin used as a loading control. (C) Quantification of triplicate plaque assays comparing parental and TgMAPK2^{AID} parasites grown in the presence and absence of IAA. Quantification of (D) invasion and (E) egress of TgMAPK2 parasites grown without and for the last 2 h with IAA. (F) Phase contrast micrograph comparing 20 h growth (-/+) IAA treatment. Arrowheads indicate individual vacuoles. Scale bars = 10 µm. p values are from two-tailed Student's t-test.

Figure 4. Loss of TgMAPK2 leads to a defect in daughter cell budding. TgMAPK2^{AID} parasites stably expressing mTFP1-α-Tubulin (magenta) and TgIMC1-mVenus (green) were stained with Hoechst 33342 (blue) to distinguish the three indicated categories in cell cycle. Scale bars: 2 µm. (B) Experimental flow of addition of IAA in increasing 2h increments. (C) Quantification of parasites in

each category with increasing time of growth in IAA. Mean of n=3 biological replicates; 200-300 parasites counted per condition. p values from one-way ANOVA with Dunnett's test. (D) Western blot demonstrates MAPK2^{AID} protein levels are restored 2-4 h after IAA washout. (E) Phase contrast micrograph comparing growth of TgMAPK2^{AID} parasites over 26 h in IAA or after 8 h in IAA with an additional 18 h after wash-out. Arrowheads indicate individual vacuoles. Scale bars = 20 µm. (F) Quantification of percent of vacuoles that appeared to be replicating normally (≥4 parasites/vacuole) of n=3 independent replicates as in (E). p values are from one-way ANOVA with Tukey's test. ($p<0.0001$: ***).

Figure 5. Prolonged incubation in IAA results in multiple defects in TgMAPK2^{AID} parasite ultrastructure. Transmission electron micrographs of intracellular TgMAPK2^{AID} parasites in (A,B) the absence of IAA, 6 h growth in IAA (C,D) or 20 h IAA (E,F and G,H). Daughter buds (*), Golgi apparatus (Go), Apicoplast (Ap), Mitochondria (Mt); Residual bodies (RB) are marked. All scale bars: 1 µm. Note that 100% of parasites treated for 20 h IAA had overduplicated apicoplasts, and 35±5% had overduplicated Golgi; neither phenotype was observed in untreated parasites.

Figure 6. Loss of TgMAPK2 does not block organelle replication. Z-projections of confocal stacks of the TgMAPK2^{AID} parasites that were allowed to invade for 2 h and then grown for 12 hours in the absence (A) or presence (B) of 500 µM IAA. Parasites were fixed and stained with DAPI (blue) and antibodies for TOM40 (red) and ACP1 (green). Scale bars: 5 µm.

Figure 7. TgMAPK2 depletion impairs centrosome duplication. (A) Z-projections of confocal stacks of TgMAPK2^{AID} parasites stably expressing mVenus-TgCentrin1 (green) and TgCEP250L1-3xHA (red) were grown for 8 hours in the presence (+) or absence (-) of 500 µM IAA, and co-stained with Hoechst (blue). TgCentrin1 (arrows), TgCEP250L1 (large arrowheads). Nuclei are outlines in yellow. Scale bars: 2 µm. (B) TgMAPKL1^{AID} or TgMAPK2^{AID} parasites expressing TgCentrin1-mVenus (green) were

treated with 500 μM IAA for 8 hours and co-stained with anti-TgIMC1 (red) and Hoechst (blue). Guide panels are a merge of Centrin-1 and IMC1 signals, numbers indicate number of centrosomes. Scale
420 bars: 5 μm.

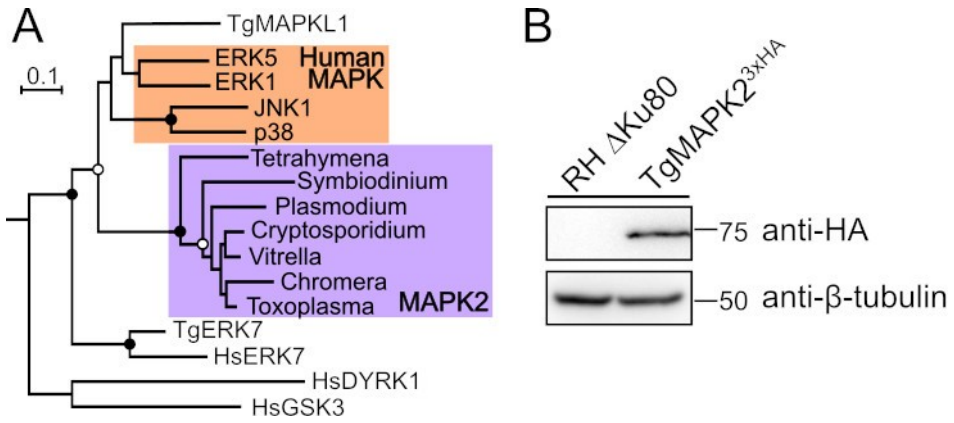

Figure 1. (A) Phylogenetic tree demonstrates MAPK2 represents a distinct MAPK subfamily (highlighted purple) that is conserved throughout Alveolata. Human MAPKs ERK1, ERK5, JNK1, and p38 are highlighted orange. Human DYRK1, GSK3, and ERK7 and *Toxoplasma* MAPKL1 and ERK7 were used as outgroups. Bootstrap support indicated by: Black circles >95%; Open circles >80%. (B) Western blot on TgMAPKL2^{3xHA} and parental lysates. β-Tubulin (anti-β-Tubulin) was used as a loading control.

Figure 2

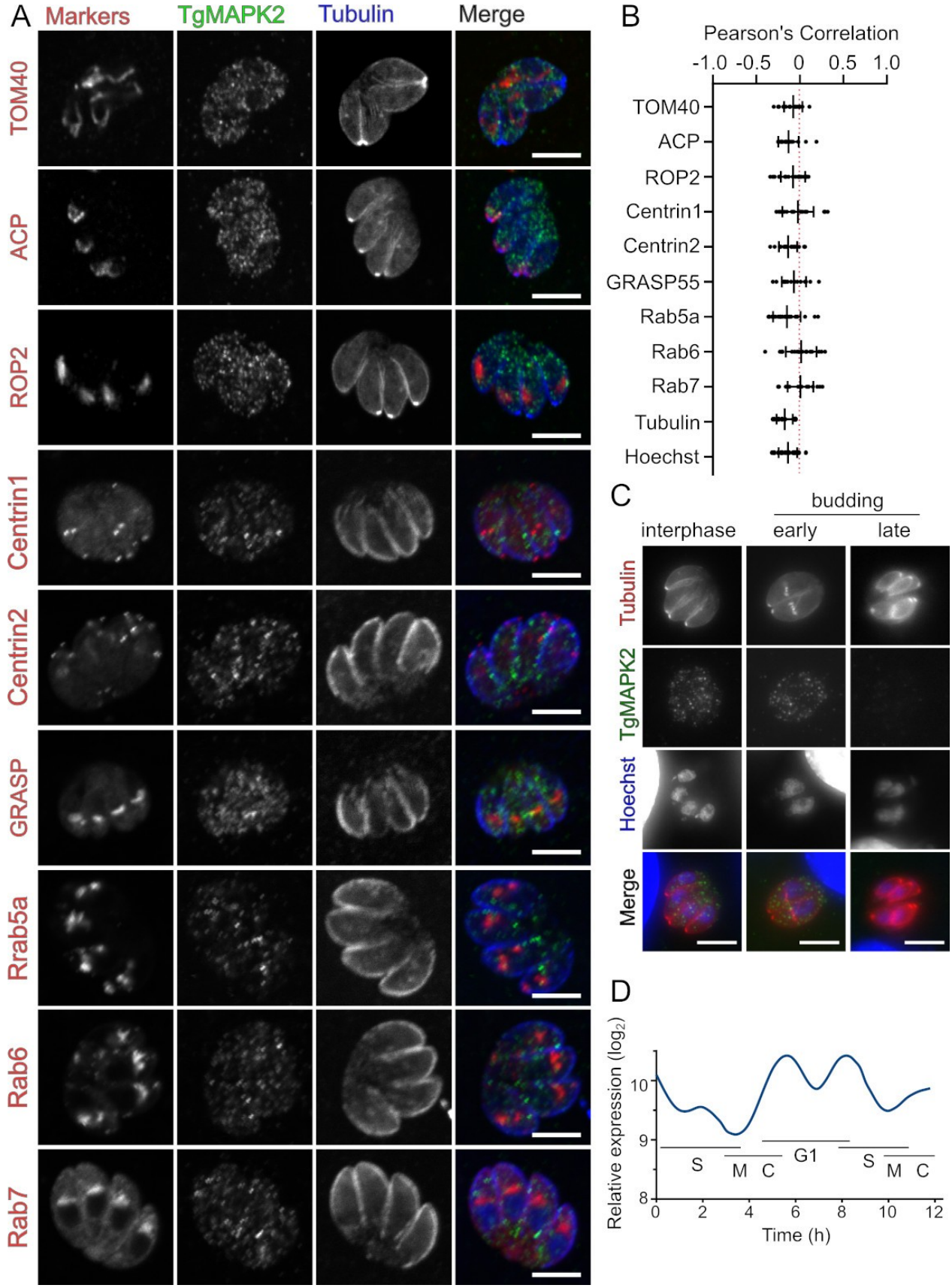
A
Markers
TgMAPK2
Tubulin
Merge
TOM40
ACP
ROP2
Centrin1
Centrin2
GRASP
Rrab5a
Rab6
Rab7
B
Pearson's Correlation
-1.0 -0.5 0 0.5 1.0
TOM40
ACP
ROP2
Centrin1
Centrin2
GRASP55
Rab5a
Rab6
Rab7
Tubulin
Hoechst
C
budding
interphase
early
late
Tubulin
TgMAPK2
Hoechst
Merge
D
Relative expression (log2)
10
9
8
S
M
C
G1
S
M
C
0 2 4 6 8 10 12
Time (h)

Figure 2. TgMAPK2 forms cytosolic puncta in interphase and early budding parasites. (A) 0.5-µm confocal slices of TgMAPK2^{3xHA} and GFP-α-Tubulin (blue) expressing parasites were either stained or transiently transfected (Centrin and Rab FP fusions) with the indicated markers. (B) Pearson's correlation coefficients for TgMAPK2^{3xHA} and the indicated markers from (A); n=20 cells. (C) TgMAPK2^{3xHA} intensity diminishes late in the cell cycle. (D) Transcript levels of MAPK2 peak during G1/early S (data (1), retrieved from ToxoDBv43). All scale bars: 5 µm.

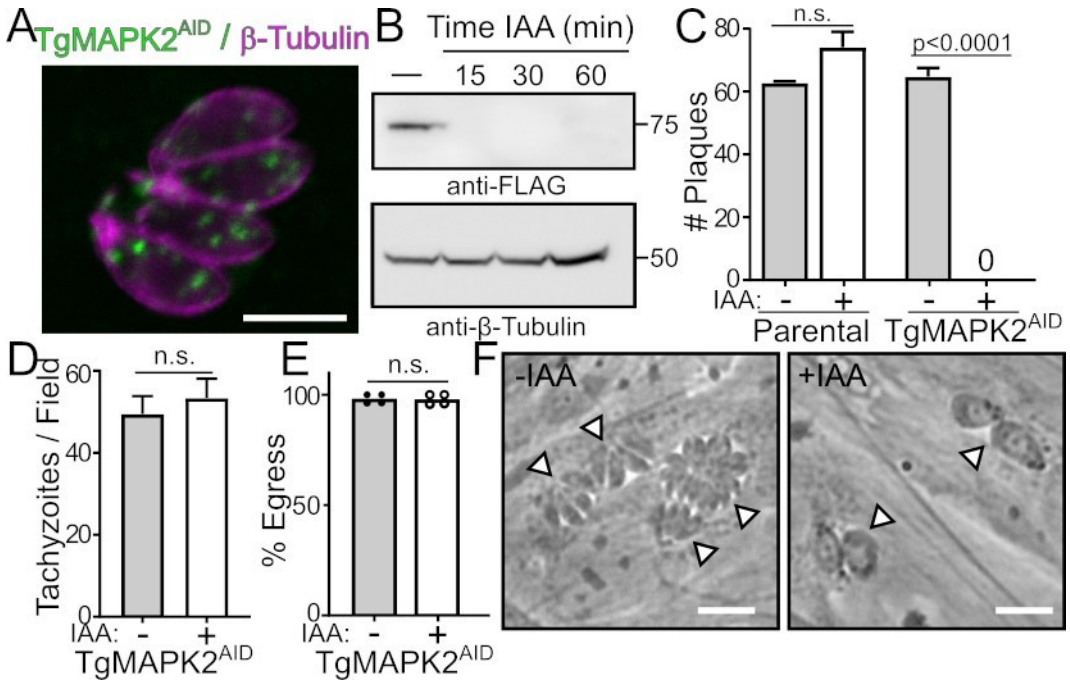

Figure 3. TgMAPK2 is essential for parasite proliferation. (A) 0.5-µm confocal slice of TgMAPK2^{AID} parasites using anti-FLAG (green) and anti-β-Tubulin (magenta). Scale bar = 5 µm. (B) Western blot of TgMAPK2^{AID} protein levels at increasing growth time in 500 µM IAA. Anti-β-tubulin used as a loading control. (C) Quantification of triplicate plaque assays comparing parental and TgMAPK2^{AID} parasites grown in the presence and absence of IAA. Quantification of (D) invasion and (E) egress of TgMAPK2 parasites grown without and for the last 2 h with IAA. (F) Phase contrast micrograph comparing 20 h growth (-/+) IAA treatment. Arrowheads indicate individual vacuoles. Scale bars = 10 µm. p values are from two-tailed Student's t-test.

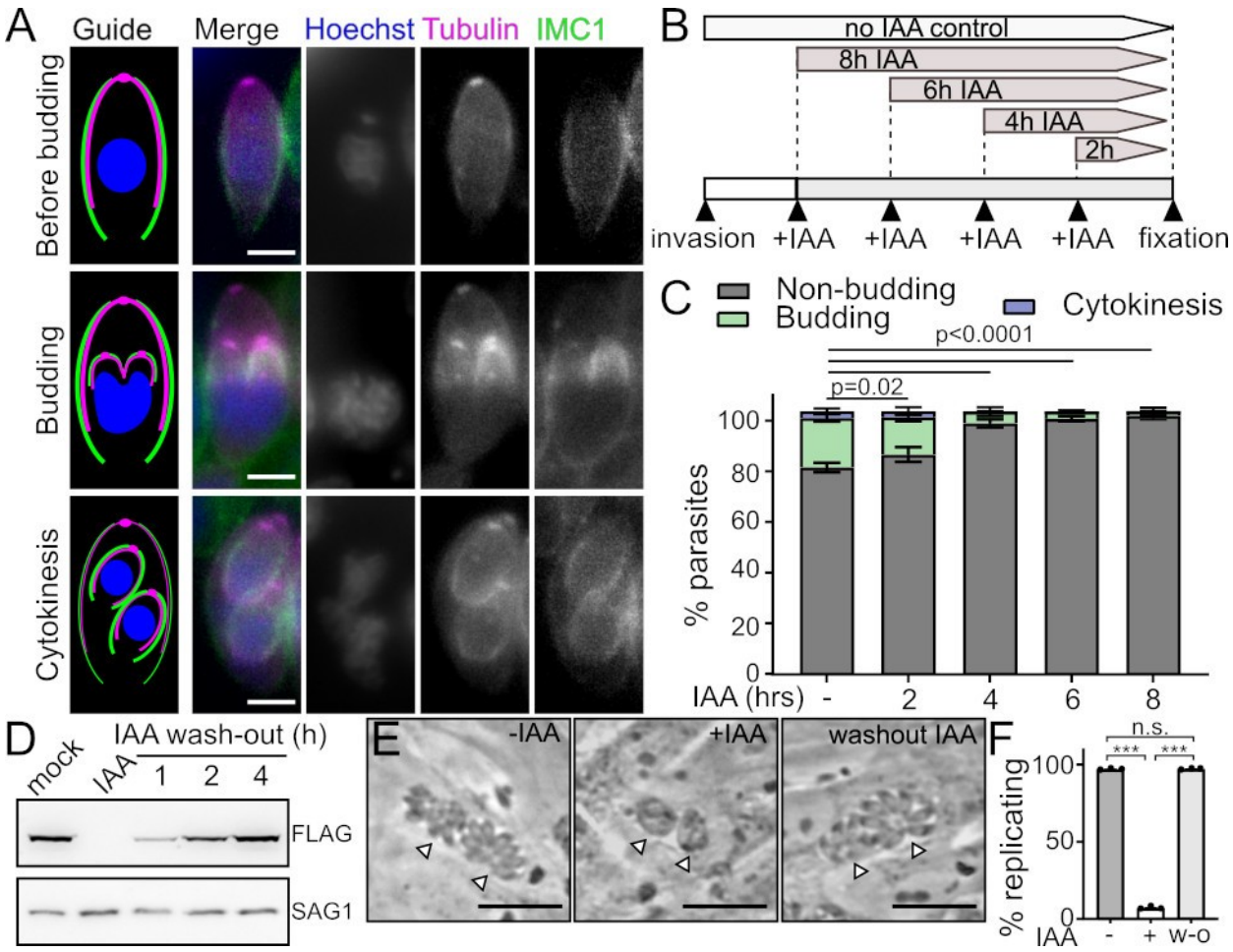

Figure 4. Loss of TgMAPK2 leads to a defect in daughter cell budding. TgMAPK2^{AID} parasites stably expressing mTFP1-α-Tubulin (magenta) and TgIMC1-mVenus (green) were stained with Hoechst 33342 (blue) to distinguish the three indicated categories in cell cycle. Scale bars: 2 µm. (B) Experimental flow of addition of IAA in increasing 2h increments. (C) Quantification of parasites in each category with increasing time of growth in IAA. Mean of n=3 biological replicates; 200-300 parasites counted per condition. p values from one-way ANOVA with Dunnett's test. (D) Western blot demonstrates MAPK2^{AID} protein levels are restored 2-4 h after IAA washout. (E) Phase contrast micrograph comparing growth of TgMAPK2^{AID} parasites over 26 h in IAA or after 8 h in IAA with an additional 18 h after wash-out. Arrowheads indicate individual vacuoles. Scale bars = 20 µm. (F) Quantification of percent of vacuoles that appeared to be replicating normally (≥4 parasites/vacuole) of n=3 independent replicates as in (E). p values are from one-way ANOVA with Tukey's test. ($p<0.0001$: ***).

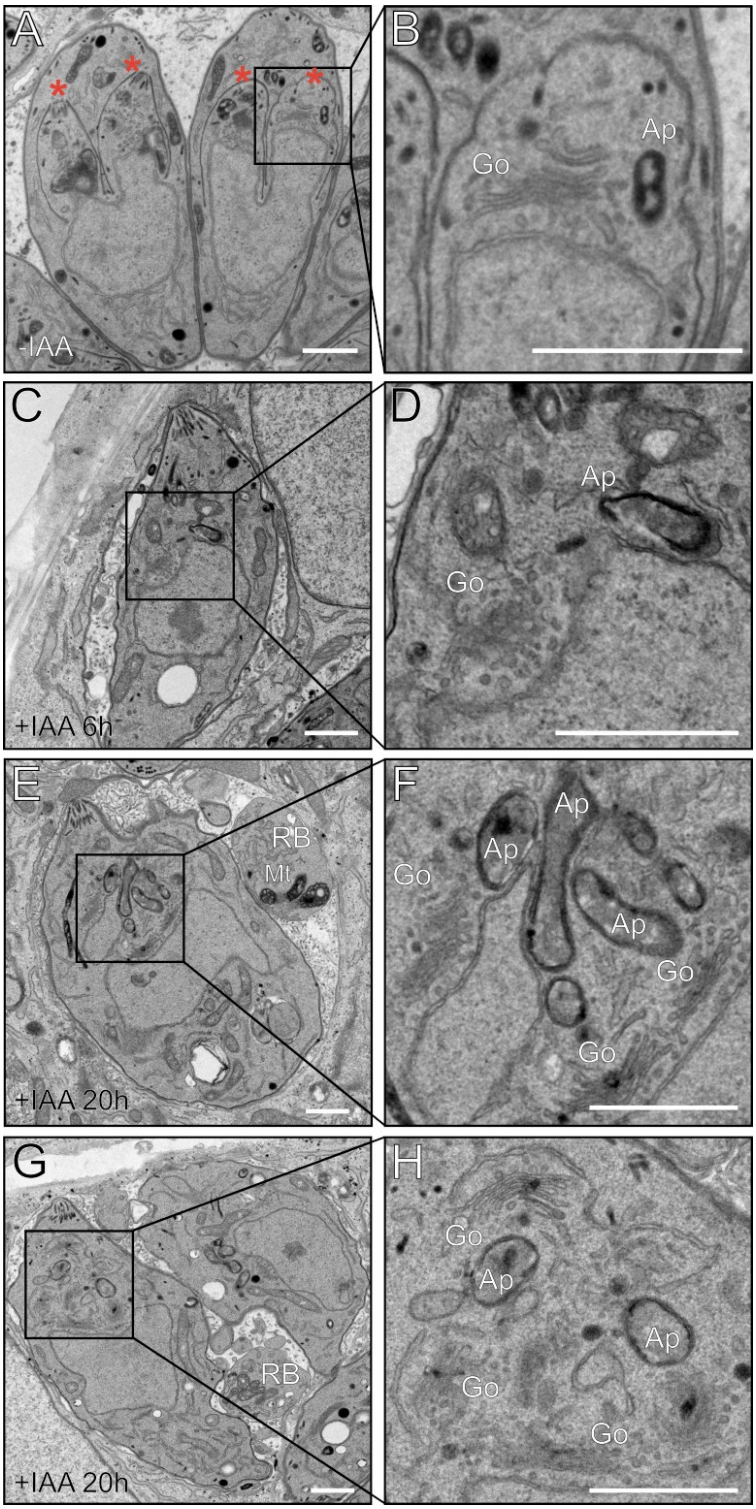

Figure 5. Prolonged incubation in IAA results in multiple defects in TgMAPK2^{AID} parasite ultrastructure. Transmission electron micrographs of intracellular TgMAPK2^{AID} parasites in (A,B) the absence of IAA, 6 h growth in IAA (C,D) or 20 h IAA (E,F and G,H). Daughter buds (*), Golgi apparatus (Go), Apicoplast (Ap), Mitochondria (Mt); Residual bodies (RB) are marked. All scale bars: 1 µm. Note that 100% of parasites treated for 20 h IAA had overduplicated apicoplasts, and 35±5% had overduplicated Golgi; neither phenotype was observed in untreated parasites.

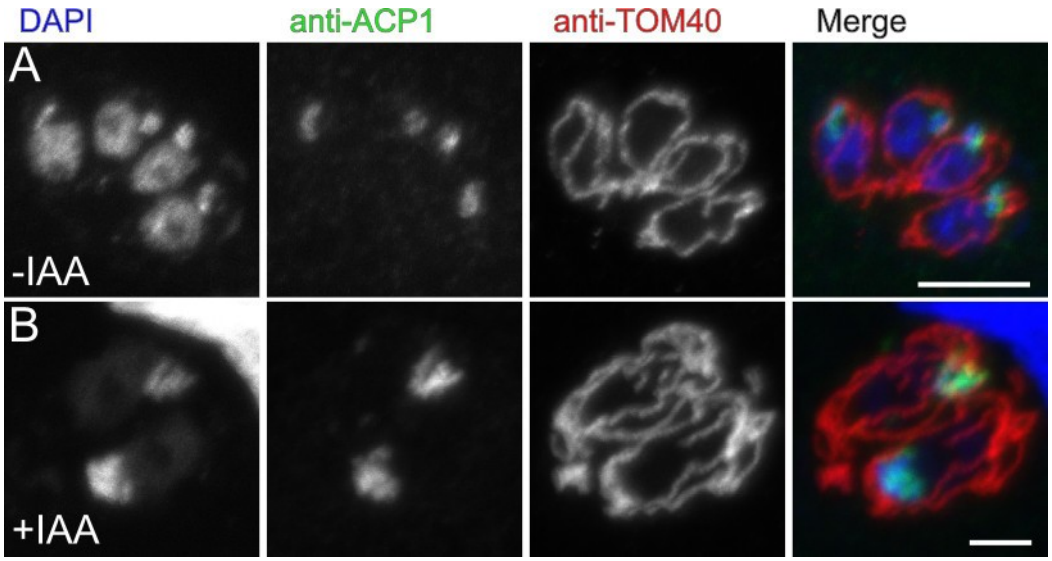

Figure 6. Loss of TgMAPK2 does not block organelle replication. Z-projections of confocal stacks of the TgMAPK2^{AID} parasites that were allowed to invade for 2 h and then grown for 12 hours in the absence (A) or presence (B) of 500 μM IAA. Parasites were fixed and stained with DAPI (blue) and antibodies for TOM40 (red) and ACP1 (green). Scale bars: 5 μm.

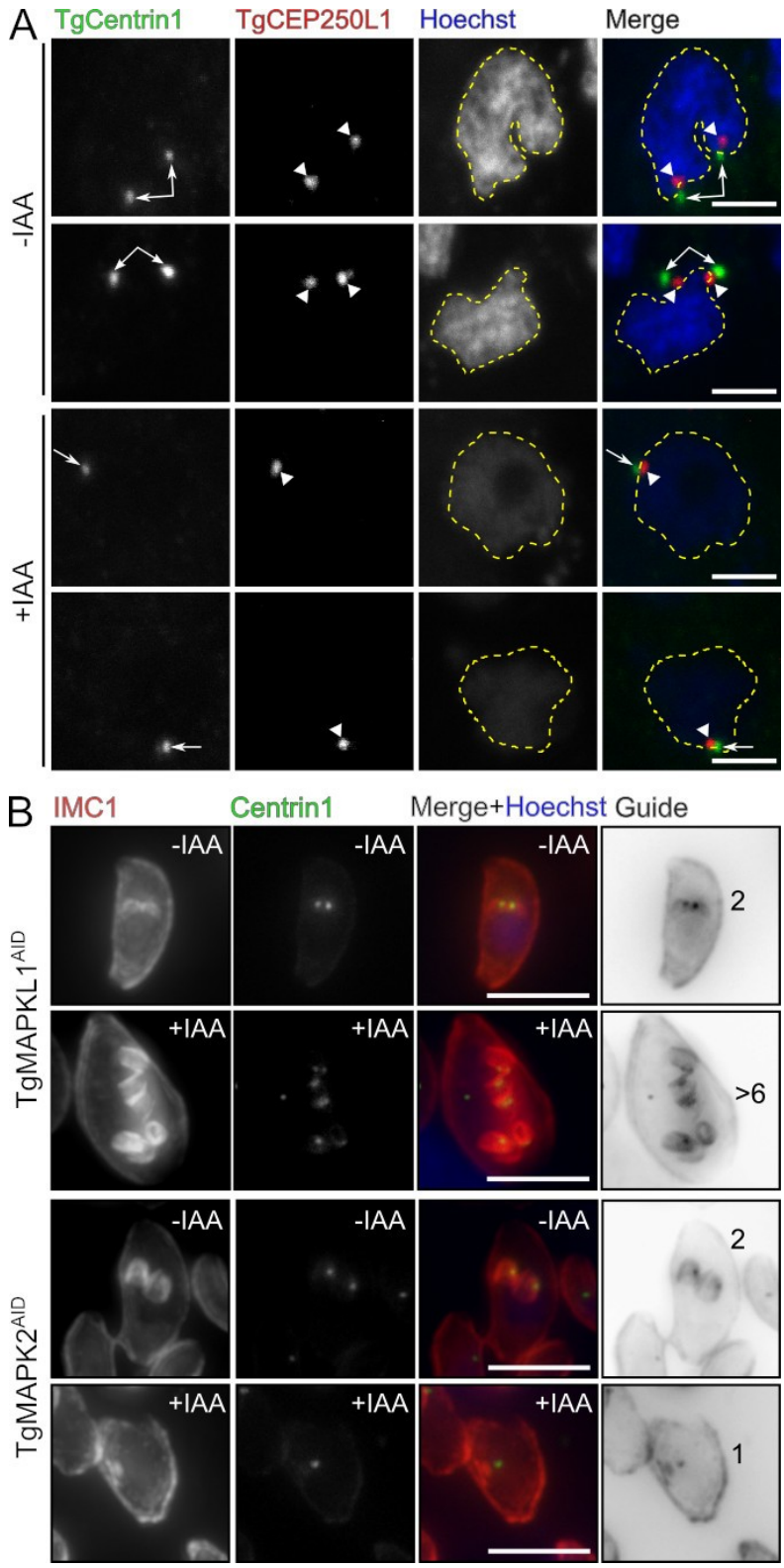

Figure 7. TgMAPK2 depletion impairs centrosome duplication. (A) Z-projections of confocal stacks of TgMAPK2^{AID} parasites stably expressing mVenus-TgCentrin1 (green) and TgCEP250L1-3xHA (red) were grown for 8 hours in the presence (+) or absence (-) of 500 µM IAA, and co-stained with Hoechst (blue). TgCentrin1 (arrows), TgCEP250L1 (large arrowheads). Nuclei are outlines in yellow. Scale bars: 2 µm. (B) TgMAPKL1^{AID} or TgMAPK2^{AID} parasites expressing TgCentrin1-mVenus (green) were treated with 500 µM IAA for 8 hours and co-stained with anti-TgIMC1 (red) and Hoechst (blue). Guide

panels are a merge of Centrin-1 and IMC1 signals, numbers indicate number of centrosomes. Scale bars: 5 μm.